Comparative study between conventional and diffusion-bonded Nd-doped vanadate crystals in the passively mode-locked operation

Y. J. Huang, Y. P. Huang, H. C. Liang, K. W. Su, Y. F. Chen[*], and K. F. Huang

Department of Electrophysics, National Chiao Tung University, Hsinchu, Taiwan
[*]yfchen@cc.nctu.edu.tw

Abstract: We design a reliable linear three-element cavity to make a comparative study between the conventional and diffusion-bonded $Nd:GdVO_4$ crystals in the passively mode-locked operation. Experimental investigations reveal that the mode-locked pulse width obtained with the diffusion-bonded crystal is considerably broader than that obtained with the conventional crystal, even though the diffusion-bonded crystal can significantly reduce the thermal effects. The pulse broadening is experimentally verified to come from the length of the undoped part that brings in a reduction of the spatial-hole-burning (SHB) effect.

@2010 Optical Society of America

OCIS codes: (140.3480) Lasers, diode-pumped; (140.3530) Lasers, neodymium; (140.4050) Mode-locked lasers; (140.6810) Thermal effects.

References and links

1. U. Keller, D. A. B. Miller, G. D. Boyd, T. H. Chiu, J. F. Ferguson, and M. T. Asom, "Solid-state low-loss intracavity saturable absorber for Nd:YLF lasers: an antiresonant semiconductor Fabry-Perot saturable absorber," Opt. Lett. **17**(7), 505–507 (1992).
2. U. Keller, K. J. Weingarten, F. X. Kärtner, D. Kopf, B. Braun, I. D. Jung, R. Fluck, C. Hönninger, N. Matuschek, and J. Aus Der Au, "Semiconductor saturable absorber mirrors (SESAM's) for femtosecond to nanosecond pulse generation in solid-state lasers," IEEE J. Sel. Top. Quantum Electron. **2**(3), 435–453 (1996).
3. U. Keller, "Recent developments in compact ultrafast lasers," Nature **424**(6950), 831–838 (2003).
4. G. J. Spühler, R. Paschotta, U. Keller, M. Moser, M. J. P. Dymott, D. Kopf, J. Meyer, K. J. Weingarten, J. D. Kmetec, J. Alexander, and G. Truong, "Diode-pumped passively mode-locked Nd:YAG laser with 10-W average power in a diffraction-limited beam," Opt. Lett. **24**(8), 528–530 (1999).
5. Y. F. Chen, S. W. Tsai, Y. P. Lan, S. C. Wang, and K. F. Huang, "Diode-end-pumped passively mode-locked high-power $Nd:YVO_4$ laser with a relaxed saturable Bragg reflector," Opt. Lett. **26**(4), 199–201 (2001).
6. L. McDonagh, R. Wallenstein, and A. Nebel, "111 W, 110 MHz repetition-rate, passively mode-locked $TEM_{00}Nd:YVO_4$ master oscillator power amplifier pumped at 888 nm," Opt. Lett. **32**(10), 1259–1261 (2007).
7. R. Paschotta, J. Aus der Au, G. J. Spühler, F. Morier-Genoud, R. Hövel, M. Moser, S. Erhard, M. Karszewski, A. Giesen, and U. Keller, "Diode-pumped passively mode-locked lasers with high average power," Appl. Phys. B **70**, S25–S31 (2000).
8. F. Hanson, "Improved laser performance at 946 and 473 nm from a composite $Nd:Y_3Al_5O_{12}$ rod," Appl. Phys. Lett. **66**(26), 3549–3551 (1995).
9. M. Tsunekane, N. Taguchi, T. Kasamatsu, and H. Inaba, "Analytical and experimental studies on the characteristics of composite solid-state laser rods in diode-end-pumped geometry," IEEE J. Sel. Top. Quantum Electron. **3**(1), 9–18 (1997).
10. Z. Zhuo, T. Li, X. Li, and H. Yang, "Investigation of $Nd:YVO_4/YVO_4$ composite crystal and its laser performance pumped by a fiber coupled diode laser," Opt. Commun. **274**(1), 176–181 (2007).
11. Y. T. Chang, Y. P. Huang, K. W. Su, and Y. F. Chen, "Comparison of thermal lensing effects between single-end and double-end diffusion-bonded $Nd:YVO_4$ crystals for $^4F_{3/2} \rightarrow {}^4I_{11/2}$ and $^4F_{3/2} \rightarrow {}^4I1_{3/2}$ transitions," Opt. Express **16**(25), 21155–21160 (2008).
12. T. Li, Z. Zhuo, S. Zhao, and Y. G. Wang, "Diode-pumped passively mode-locked $YVO_4/Nd:YVO_4$ composite crystal laser with $LT-In_{0.25}Ga_{0.75}As$ saturable absorber," Laser Phys. Lett. **5**(5), 350–352 (2008).
13. Z. Zhuo, T. Li, and Y. G. Wang, "Passively mode-locked $YVO_4/Nd:YVO_4$ composite crystal laser with a semiconductor saturable absorber as a high reflector," Laser Phys. Lett. **5**(6), 421–424 (2008).
14. B. E. Bouma, and J. G. Fujimoto, "Compact Kerr-lens mode-locked resonators," Opt. Lett. **21**(2), 134–136 (1996).
15. B. E. Bouma, M. Ramaswamy-Paye, and J. G. Fujimoto, "Compact resonator designs for mode-locked solid-state lasers," Appl. Phys. B **65**(2), 213–220 (1997).

16. B. Y. Zhang, G. Li, M. Chen, Z. G. Zhang, and Y. G. Wang, "Passive mode locking of a diode-end-pumped Nd:GdVO$_4$ laser with a semiconductor saturable absorber mirror," Opt. Lett. **28**(19), 1829–1831 (2003).
17. J. Kong, D. Y. Tang, S. P. Ng, B. Zhao, L. J. Qin, and X. L. Meng, "Diode-pumped passively mode-locked Nd:GdVO$_4$ laser with a GaAs saturable absorber mirror," Appl. Phys. B **79**(2), 203–206 (2004).
18. S. J. Zhang, E. Wu, H. F. Pan, and H. P. Zeng, "Passive mode locking in a diode-pumped Nd:GdVO$_4$ laser with a semiconductor saturable absorber mirror," IEEE J. Quantum Electron. **40**(5), 505–508 (2004).
19. G. J. Spühler, S. Reffert, M. Haiml, M. Moser, and U. Keller, "Output-coupling semiconductor saturable absorber mirror," Appl. Phys. Lett. **78**(18), 2733–2735 (2001).
20. Y. X. Fan, J. L. He, Y. G. Wang, S. Liu, H. T. Wang, and X. Y. Ma, "2-ps passively mode-locked Nd:YVO$_4$ laser using an output-coupling-type semiconductor saturable absorber mirror," Appl. Phys. Lett. **86**(10), 101103 (2005).
21. C. J. Flood, D. R. Walker, and H. M. van Driel, "Effect of spatial hole burning in a mode-locked diode end-pumped Nd:YAG laser," Opt. Lett. **20**(1), 58–60 (1995).
22. B. Braun, K. J. Weingarten, F. X. Kärtner, and U. Keller, "Continuous-wave mode-locked solid-state lasers with enhanced spatial hole burning," Appl. Phys. B **61**(5), 429–437 (1995).

1. Introduction

Diode-end-pumped passively mode-locked all-solid-state lasers with semiconductor saturable absorber mirrors (SESAMs) [1,2] have been extensively studied due to their short pulse duration, compactness, low insertion loss, flexibility, inexpensive, reliable operation, and wide bandgap ranging from visible to infrared etc. High-power mode-locked lasers are desirable because they are useful for numerous applications such as laser-video display, medicine, material processing, nonlinear wavelength conversion and so on [3]. Although several high-power passively mode-locked lasers have been proposed [4–6], thermal effects of the gain media are still the main challenge [7].

The composite crystal, which is fabricated by the diffusion bonding of a doped crystal to an undoped crystal as a heat sink for the pump surface, has been confirmed to be a superior method in reducing the thermal effects [8–11]. Recently, passively mode-locked composite crystal lasers have been reported with average output power greater than 10 W, indicating that the composite crystals are suitable for accomplishing high-power mode-locked laser [12,13]. Nevertheless, so far there is no systematic comparison between the conventional and composite crystals in the passively mode-locked performance.

In this work, we develop a linear three-element resonator to make a comparative study between the conventional crystal (Nd:GdVO$_4$) and the composite crystal (GdVO$_4$/Nd:GdVO$_4$) in the passively mode-locked performance. Compared to the conventional Nd:GdVO$_4$ crystal, the maximum output power with the diffusion-bonded Nd:GdVO$_4$ crystal can be enhanced by nearly 30% thanks to the reduction of thermal effects. However, the mode-locked pulse widths obtained with the diffusion-bonded crystal are found to be considerably broader than that obtained with the convenient crystal. We experimentally confirm that the undoped part of the diffusion-bonded crystal introduce a reduction of the spatial-hole-burning (SHB) effect to lead to the pulse broadening. Our experimental results reveal that the length of the undoped part needs to be taken into account in optimizing the pulse width of the mode-locked laser.

2. Cavity design and analysis

First of all we design a reliable cavity to evaluate the mode-locked laser performance between the conventional crystal and the composite crystal. In the past years, the three-element resonator, consisting of a flat rear mirror, a convex lens and a flat output coupler, has been identified to be an effective method for realizing the Kerr-lens mode-locked laser [14,15]. The linear three-element resonator is beneficial for easy assembly, mode-matching design, and insensitivity to misalignment. Moreover, the linear three-element resonator is also practically useful for the evaluation of thermal effects in the laser crystal. Therefore, here we employ the linear three-element resonator to design a passively mode-locked laser with SESAM as a saturable absorber for studying the performance between the conventional crystal and the composite crystal.

The configurations for a three-element cavity with and without the thermal-lensing effect are shown in Fig. 1(a) and 1(b), where L_1 is the distance between the front mirror and the convex lens, L_2 is the distance between the convex lens and the output coupler, and f is the

focal length of the convex lens. The laser crystal and the SESAM device are designed to be as close as to the front mirror and the output coupler, respectively. With a pump spot radius of 100 μm, the mode size at the front mirror ω_1 is aimed at 160 μm to lead to a good mode-size matching. On the other hand, the mode size at the output coupler ω_2 is aimed to be 50 μm to achieve a high-quality mode-locked operation. Consequently, the required mode-size ratio ω_1/ω_2 is approximately 3.2. The focal length of the convex lens is chosen to be $f = 125$ mm. The key issue for the cavity design is to determin the values of L_1 and L_2.
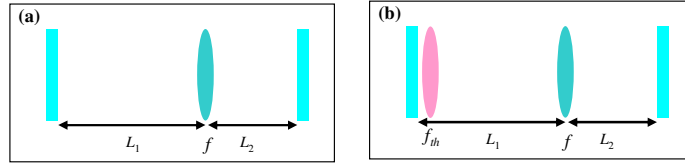

Fig. 1. The configurations for a three-element cavity (a) with and (b) without the thermal-lensing effect.

Using the ABCD-matrix method, the stable condition for a three-element cavity without the thermal-lensing effect is given by $0 \le (1 - L_1/f)(1 - L_2/f) \le 1$. For the purpose of presentation, we define the factor $\eta = 1/(1 + \omega_1/\omega_2)$ and calculate η with $f = 125$ mm as a function of L_1 and L_2. In Fig. 2, a rainbow color bar is used to present the different value of the calculated η, whereas the unstable zone is displayed with a black color. The stable region can be clearly seen to be enclosed by three curves: $(1 - L_1/f)(1 - L_2/f) = 1$, $L_1 = f$, and $L_2 = f$. For the required ratio of $\omega_1/\omega_2 = 3.2$, the corresponding η value is 0.238 that is characterized by a light pink in the color bar. With the representation of Fig. 2, the appropriate values of L_1 and L_2 can be found to approximately 500 mm and 166 mm, respectively, as the location of point P indicated in Fig. 2.
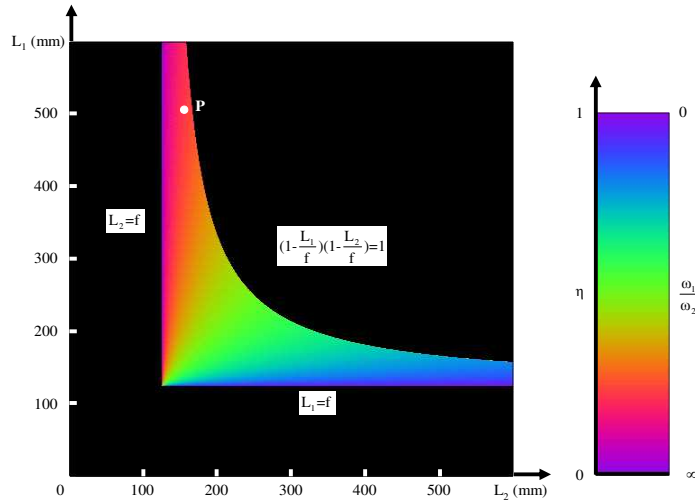

Fig. 2. Calculated results for the factor η as a function of L₁ and L₂ with $f = 125$ mm; the black color denotes the unstable zone.

Taking the thermal-lensing effect into account, we find that the effective focal power of the thermal lens in the laser crystal needs to be smaller than $2(L_1 - f)^{-1}$ to maintain the cavity stable. With $L_1 = 500$ mm and $f = 125$ mm, we can find that the critical focal length of the thermal lens is approximately 188 mm. The focal length of the thermal lens can be expressed as $f_{th} = C\omega_p^2/P_{in}$ [11], where ω_p is the pump radius on the gain medium, P_{in} is the incident

pump power, and C is a proportional constant. As a result, we can calculate the critical pump power $P_{critical}$ beyond which the thermal-lensing effect will cause the cavity to be unstable. It is clear that the smaller thermal-lensing effect the laser crystal brings in, the higher critical pump power can be reached.

3. Experimental setup

The experimental setup is schematically shown in Fig. 3. The laser cavity contains a gain medium, a convex lens, and an output-coupling semiconductor saturable absorber mirror (SESAMOC). The gain medium is a Nd:GdVO$_4$ crystal that owns high absorption coefficient for diode pumping, large stimulated emission cross section, and high thermal conductivity along the <110> direction [16–18]. We prepared two types of gain media for the purpose of our experimental study. The one was a conventional 0.5 at.% Nd:GdVO$_4$ crystal with dimensions of $3 \times 3 \times 8$ mm^3, the other one was a $3 \times 3 \times 10$ mm^3 composite GdVO$_4$/Nd:GdVO$_4$ crystal with a 2-mm-long undoped GdVO$_4$ crystal diffusion bonded to a 0.5 at.% Nd:GdVO$_4$ crystal. The pump facets of two type of laser crystals were coated at 808 nm for high transmission as well as at 1064 nm for high reflection (HR) as rear mirrors, and the other sides of each were anti-reflection (AR) coated at 1064 nm and wedged 0.5° to suppress the Fabry-Perot etalon effect. The laser crystals were wrapped with indium foil and mounted in a copper holder with water-cooled at 20 °C. The pump source was a 10-W 808-nm fiber-coupled laser diode with a core radius of 100 μm and a numerical aperture of 0.16. The pump beam was re-imaged into the laser crystal with a lens set that has a focal length of 25 mm with a magnification of unity and a coupling efficiency of 85%. The convex lens with focal length of 125 mm was anti-reflective at 1064 nm on both sides.
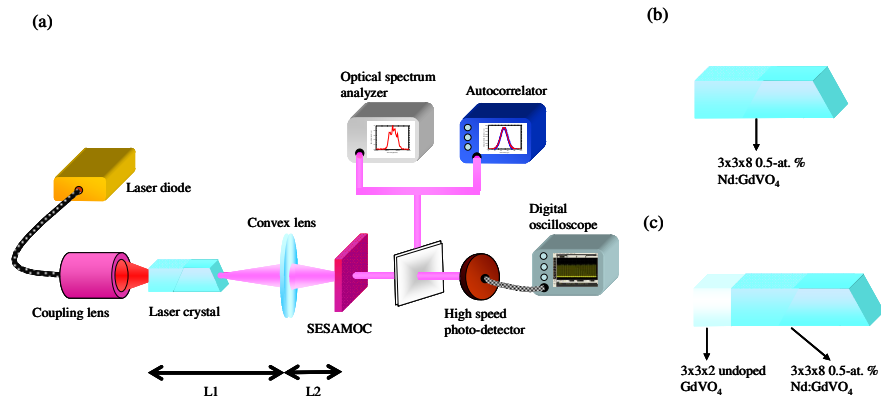

Fig. 3. (a) Schematic of a linear three-element diode-end-pumped passively mode-locked laser; (b) conventional Nd:GdVO$_4$ crystal; (c) composite GdVO$_4$/Nd:GdVO$_4$ crystal.

For passively mode-locked operation at 1064 nm, we fabricated a SESAM structure that was monolithically grown on an undoped GaAs substrate by metalorganic chemical vapor deposition (MOCVD). The present SESAM device was designed to simultaneously serve as an saturable absorber and an output coupler (SESAMOC) [19,20]. The saturable absorber was composed of two 8-nm In$_{0.34}$Ga$_{0.66}$As quantum wells (QWs) with a modulation depth of 1.5% and a saturable fluence of 80 μJ/cm^2. The Bragg mirror structure comprised 10 AlAs/GaAs quarter-wavelength layers, designed for a reflectivity of 96.3% at 1064 nm. The back side of the 350-μm GaAs substrate was coated for anti-reflection at 1064 nm. The SESAMOC was surfaced mounted in a copper without any active cooling. As designed in Sec. 2, L_1 and L_2 were set at 500 mm and 166 mm, respectively, to implement the mode-locked operation. The total cavity length was then 666 mm, corresponding to repetition rates of 225 MHz. The mode radii on the laser crystal and the SESAMOC were approximately 160 μm and 50 μm, respectively. The cw mode-locked pulses were detected by a high-speed InGaAs photodetector (Electro-optics Technology Inc. ET-3500 with rise time 35 ps), whose output

signal was connected to a digital oscilloscope (Agilent, DSO 80000) with 12 GHz electrical bandwidth and the sampling rates of 25 ps. The spectral information of the laser was monitored by a Fourier optical spectrum analyzer (Advantest, Q8347) that is constructed with a Michelson interferometer with resolution of 0.003 nm.

4. Results and discussion

The dependence of average output power on the incident pump power is shown in Fig. 4(a). The slope efficiencies obtained with the conventional and composite gain media were found to be almost the same, approximately 35%. The threshold pump powers for the cw mode-locked operation were also very comparable for two types of gain media, approximately to be 1.7 W. When the pump power exceeded 1.7 W, the stable mode-locked pulses could be continuously generated, as shown in Fig. 4 (b). The thermal lensing effect leads to a critical pump power that restricts the maximum TEM_{00} output power in the cw mode-locked operation. When the pump power exceeded the critical pump power, the pulse train was found to be unstable, as revealed in Fig. 4(c). The critical pump powers were approximately 5.4 W and 7.8 W for the cavities with the conventional and composite gain media, respectively, as shown in Fig. 4(a). Limited by the thermal lensing effect, the maximum output powers were 1.75 W and 2.30 W for the cavities with the conventional and composite gain media, respectively. In short, the maximum output power with the diffusion-bonded crystal can be enhanced by nearly 30% thanks to the reduction of thermal effects.
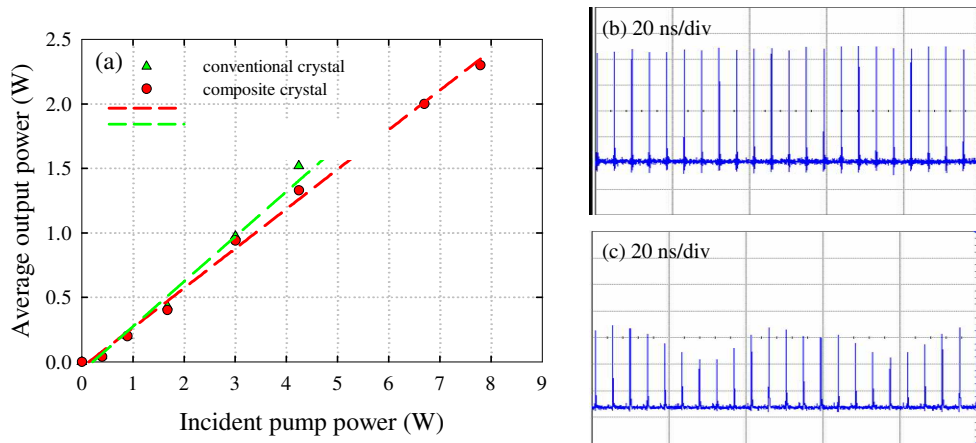

Fig. 4. (a) Average output power at 1064 nm versus incident pump power in cw mode-locked operations. And pulse trains on two circumstances with time span of 200 ns: (b) Stable cw mode-locked pulse train; (c) Modulation mode-locked pulse train with 24-MHz fluctuation.

With the help of the commercial autocorrelator (APE pulse check, Angewandte physik & Elektronik GmbH), we measured the full width at half maximum (FWHM) of the autocorrelation trace of the mode-locked pulse. Assuming the $sech^2$-shaped temporal profile, the pulse widths were found to be 8.0 ps and 24 ps for the cavities with the conventional and composite gain media, respectively, as shown in Fig. 5(a) and 5(b). We also measured the optical spectra for the mode-locked laser outputs. The FWHM of the optical spectra was found to be 0.17 nm and 0.07 nm for the cavities with the conventional and composite gain media, respectively, as shown in Fig. 6(a) and Fig. 6(b). It can be seen that the pulse broadening is consistent with the narrowing of the optical spectrum for the cavity with a composite crystal. Therefore, it is worthwhile to explore the origin of spectral narrowing in the cavity with a composite gain medium. In the following, we will verify that the undoped part of the diffusion-bonded crystal introduce a reduction of the SHB effect to lead to the spectral narrowing.
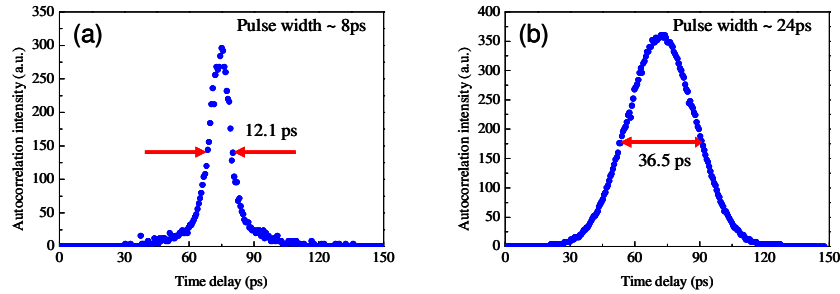
Fig. 5. Autocorrelation traces of the output pulses from (a) cw mode-locked Nd:GdVO$_4$ laser and (b) cw mode-locked GdVO$_4$/Nd:GdVO$_4$ laser;
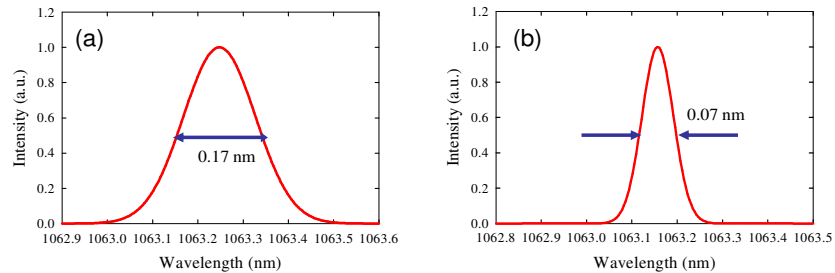

Fig. 6. Optical spectrum for (a) cw mode-locked Nd:GdVO$_4$ laser and (b) cw mode-locked GdVO$_4$/Nd:GdVO$_4$ laser.

The influence of the SHB effect on the performance of mode-locked solid-state lasers was previously studied for the cases of gain-at-the-end (GE), gain-in-the-middle (GM) as well as the intermediate transition between GE and GM [21,22]. It was found that thanks to the enhancement of the SHB effect, the pulse width in a GE mode-locked laser could be shorter than that in a GM mode-locked laser under the same cavity configuration. To investigate the SHB effect in the present three-element cavity, we replaced the HR-AR coated gain medium with a AR-AR coated Nd:GdVO$_4$ crystal and a flat front mirror. We then used a linear micro-stage to tailor the degree of the SHB effect by varying the separation d between the gain medium and the front mirror. With increasing the separation d from $d = 0.2$ mm to $d = 10$ mm, we found that the mode-locked pulse increased smoothly from 15.8 ps to 36.6 ps and the optical spectral FWHM changed from 0.085 nm to 0.048 nm, as shown in Fig. 7. In short, the pulse width strongly depends on the separation between the gain medium and the front mirror. The effective optical length of the undoped part in the diffusion-bonded crystal was approximately 4.5 mm. Referring to the results in Fig. 7, such a separation could cause the lasing spectral width to be significantly narrowed; consequently, the pulse width would be nearly doubled. This result is consistent with the experimental observation in the mode-locked laser with a composite crystal as a gain medium. Therefore, it is practically important in optimizing the mode-locked pulse width to consider the influence of the undoped length of the composite crystal.
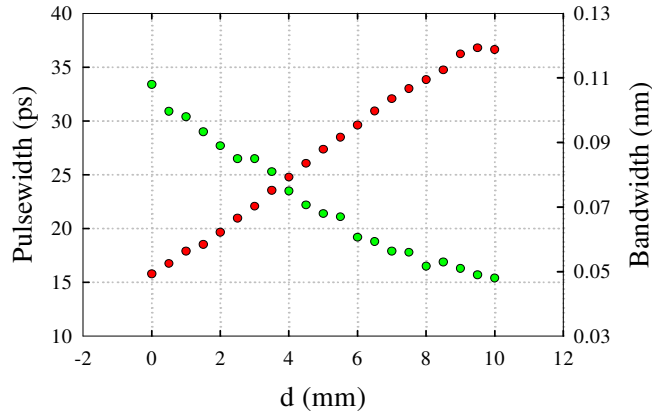
Fig. 7. Pulse width (red) and spectral FWHM (green) as a function of the Nd-doped gain medium/front mirror separation *d*.

5. Conclusion

In conclusion, a comparative study between the conventional and diffusion-bonded Nd:GdVO$_4$ crystals in the passively mode-locked operation has been performed by designing a reliable linear three-element cavity. We have found that although the diffusion-bonded crystal can usefully reduce the thermal effects, the mode-locked pulse width is usually broader than that obtained with the conventional crystal. To explain the experimental results, we have experimentally built the relationship between the degree of the SHB effect and the separation between the gain medium and the front mirror. With the developed relationship, we confirm the origin of the pulse broadening in the mode-locked laser with a composite crystal. Our investigations also indicate that the specification of the undoped length in the composite crystal needs to take into account for optimizing the mode-locked pulse width.

Acknowledgments